Progress and Developments of Downburst Prediction Applications of GOES

KENNETH L. PRYOR

NOAA/NESDIS/Center for Satellite Applications and Research, College Park, Maryland

(Manuscript received 4 September 2014, in final form 22 June 2015)

ABSTRACT

The National Environmental Satellite, Data, and Information Service (NESDIS) Center for Satellite Applications and Research (STAR) has developed and evaluated a suite of products that assess convective storm–generated downburst potential derived from *Geostationary Operational Environmental Satellite-13–15* (*GOES-13–15*). The existing suite of downburst prediction algorithms employs the GOES sounder to calculate risk based on conceptual models of favorable environmental thermodynamic profiles for downburst occurrence. A diagnostic nowcasting product, the Microburst Windspeed Potential Index (MWPI), is designed to identify attributes of a favorable downburst environment: 1) the presence of large CAPE and 2) the presence of a surface-based or elevated mixed layer with a large temperature lapse rate. This paper provides an updated assessment of the MWPI algorithm, presents case studies demonstrating effective operational use of the MWPI product, and presents validation results for the Great Plains and mid-Atlantic coastal region of the United States. MWPI data were collected for downburst events that occurred during the convective seasons of 2007–13 and were validated against surface observations of convective wind gusts as recorded by wind sensors in high quality mesonetworks over the southern Great Plains and the Chesapeake Bay region. Favorable validation results include a correlation greater than 0.6 and low mean error [<0.1 knot (kt; where $1\,\text{kt} = 0.51\,\text{m}\,\text{s}^{-1}$)] between MWPI values and measured confirmed downburst wind speeds over contrasting climate regions of the continental United States. Case studies over the mid-Atlantic region and northern Florida highlight the adaptability of the MWPI algorithm to severe convective storm forecasting and warning operations.

1. Introduction

Convective storms that are capable of producing intense downdrafts and resulting strong outflow winds at or near the surface have been identified as a serious hazard for aircraft during takeoff and landing and marine transportation, especially passenger vessels and vessels under sail. Fujita (1985) and Wakimoto (1985) define a downburst, in general, as a strong downdraft that induces an outburst of damaging winds at or near the ground, and a microburst as a very small downburst with an outflow diameter of less than 4 km and a lifetime of less than 5 min. Ellrod et al. (2000) noted that between 1975 and 1994, 21 fatal downburst-related aircraft accidents were documented by the National Transportation Safety Board (NTSB). Since 1994, the NTSB has documented 10 downburst-related fatal aircraft accidents, mostly involving general aviation flights in the continental United States (CONUS). In addition, since 2000, significant downburst-related marine transportation accidents have been documented. Two noteworthy accidents include the fatal capsize of the passenger vessel *Lady D* in the Baltimore, Maryland, harbor in March 2004 (National Transportation Safety Board 2006), and the capsizing and sinking of the Canadian sailing vessel *Concordia* off the coast of Brazil in February 2010 (Transportation Safety Board of Canada 2010). Despite the general reduction in the frequency of downburst-related aviation accidents, the continued occurrence of passenger marine transportation accidents and fatal general aviation accidents due to downbursts within the last decade warrants the ongoing development and refinement of techniques and products designed for the short-term prediction of downburst potential. Downburst potential products derived from *Geostationary Operational Environmental Satellite-13–15* (*GOES-13–15*) sounder data have been developed and evaluated. This study entails recent modification, validation, and application of an algorithm that capitalizes on improvements to the GOES sounding process to extend the predictability

Corresponding author address: Kenneth Pryor, Satellite Meteorology and Climatology Division, Operational Products Development Branch, NOAA/NESDIS/E/RA, NCWCP, Rm. 2833, 5830 University Research Ct., College Park, MD 20740.
E-mail: ken.pryor@noaa.gov

DOI: 10.1175/WAF-D-14-00106.1

TABLE 1. Comparison of the WMSI and MWPI algorithms.

	WMSI	MWPI
Definition	$\equiv(\text{CAPE} \times \Delta\theta_e)/1000\,\text{J kg}^{-1}$	$\equiv(\text{CAPE}/1000\,\text{J kg}^{-1}) + \{\Gamma/5°\text{C km}^{-1} + [(T - T_d)_{850} - (T - T_d)_{670}]/5°\text{C}\}$
Environment	Wet/humid	Hybrid/intermediate
Reference	Atkins and Wakimoto (1991); Pryor and Ellrod (2004a,b)	Pryor (2010, 2012, 2014)

of downburst-generated winds, especially to intermediate environments between humid and arid extremes.[1]

The existing GOES sounder–derived microburst products are designed to diagnose risk based on favorable environmental thermodynamic profiles for severe convective storm development. Menzel et al. (1998) describe the role, performance, and weather forecasting applications of the current generation of GOES sounders, as well as the thermodynamic profile generation process. The typical horizontal scale of a single-cell convective storm or larger downburst (or macroburst) is near 10 km (Byers and Braham 1949). Considering the 10-km spacing of sounding retrievals, the GOES sounder is well suited to observe horizontal variations in environmental conditions and associated parameters that indicate risk of strong winds produced by downbursts. In addition, a new version of the sounding physical retrieval algorithm (Li et al. 2008) was implemented into GOES operations in 2011. This new version includes a number of improvements: 1) use of regression-retrieved temperature and moisture vertical profiles, 2) use of an error covariance matrix of the retrieval parameters, 3) application of a new radiance bias adjustment scheme, 4) use of the Pressure-Layer Fast Algorithm for Atmospheric Transmittance (PFAAST) models to calculate sounder radiances, and 5) most importantly, employment of a synthetic regression-based surface emissivity scheme. The regression-based emissivity scheme is derived from the SeeBor training database in which surface emissivity is applied to the IR regression retrieval of atmospheric moisture profiles using radiances from MODIS. Improvement is shown over retrievals made with the typical assumption of constant emissivity (Seeman et al. 2008).

Pryor and Ellrod (2004a,b) outlined the development of a suite of GOES sounder–derived products to assess the presence of conditions favorable for dry and wet microbursts. That study introduced the wet microburst severity index (WMSI) product to calculate the potential magnitude of convective downbursts in humid environments over the eastern United States. The WMSI, as outlined in Table 1, incorporated (surface based) convective available potential energy (CAPE) as well as the vertical equivalent potential temperature difference $\Delta\theta_e$ between the surface and midtroposphere (Atkins and Wakimoto 1991). Large $\Delta\theta_e$ values imply the presence of midtropospheric unsaturated air that may result in evaporative cooling and the generation of large negative buoyancy as the dry air is entrained into the convective downdraft. However, more recently, James and Markowski (2010), based on numerical simulations, found that dry air aloft had a detrimental effect on convective intensity that resulted in a reduction in hydrometeor mass, especially a decrease in hail generation. This effect was explored for a range of wind shear from 10 to 17.5 m s^{-1} over the lowest 2.5 km of the base-state profile. The reduced hail mixing ratio and resulting reduction in hail melting rate was a factor in the offset of the favorable effects of dry air aloft for downdraft development. The overall effect of dry air aloft was to reduce downdraft mass flux and cold-pool strength in low-to-moderate CAPE environments. Complementary to the results of James and Markowski (2010), a poor correlation r between $\Delta\theta_e$ and downburst magnitude will be shown in this paper.

Johns and Doswell (1992) identified necessary ingredients for deep convection: 1) a layer of high relative humidity of sufficient depth in the low or midtroposphere, 2) a steep lapse rate to allow for a substantial positive area or CAPE, and 3) sufficient lifting of a parcel from the moist layer to allow it to reach its level of free convection (LFC). CAPE has an important role in precipitation formation because of the strong dependence of updraft strength and resultant storm precipitation content on positive buoyant energy. Condensate loading (Srivastava 1985, 1987), sometimes combined with the entrainment of subsaturated air in the storm middle level (Knupp 1989), initiates the convective downdraft. The subsequent melting of frozen hydrometeors and subcloud evaporation of liquid precipitation, in conjunction with precipitation loading, result in the cooling and negative buoyancy that accelerate the downdraft in the unsaturated layer (Srivastava 1987). Collectively,

[1] An earlier version of this work was presented at the Asia–Pacific Remote Sensing Symposium's Conference on Remote Sensing of the Atmosphere, Clouds, and Precipitation V (Pryor 2014).

melting of ice-phase precipitation, subsequent evaporative cooling, and the resulting downdraft strength are enhanced by large liquid water content and the related water surface available for evaporation, and a large lapse rate that acts to maintain negative buoyancy as the downdraft descends in the subcloud layer (Srivastava 1985, 1987). The intense downdraft subsequently produces strong and potentially damaging winds upon impinging on the surface. Ellrod (1989) noted that lapse rates, specifically between 700 and 850 mb, contained the most predictive information for determining downburst potential using GOES sounder thermodynamic profile data. Thus, considering the results presented by Srivastava (1987), Caracena and Flueck (1988), and James and Markowski (2010), environmental factors that result in convective storm downdraft acceleration in the lower troposphere, including the melting and subcloud layers, are important for further consideration.

The absolute value of the temperature lapse rate[2] $|\Gamma|$ and the dewpoint depression difference ΔDD between two levels as predictors effectively indicate a favorable lower-tropospheric thermodynamic (high cloud base) environment with large values of dewpoint depression at the surface (Srivastava 1987; Caracena and Flueck 1988). Caracena and Flueck (1988) noted that the majority of microburst days during the Joint Airport Weather Studies (JAWS) project conducted in the Denver, Colorado, area were characterized by environments intermediate between the dry and wet extremes (i.e., ''hybrid''). In a prototypical dry microburst environment, Wakimoto (1985) identified a convective cloud-base height near 500 mb associated with an inverted-V thermodynamic profile. In contrast, Atkins and Wakimoto (1991) identified that a typical cloud-base height in a wet microburst environment is near the 850-mb level. Thus, a cloud-base height of 670 mb was proposed for a hypothetical hybrid microburst environment. Pryor (2012) outlined the selection process for the upper boundary level of 670 mb for a microburst wind speed potential calculation that agreed well with the mean convective cloud-base height of 685 mb inferred from the inspection of 51 GOES proximity soundings corresponding to downburst events that occurred in Oklahoma and western Texas between 1 June 2007 and 31 August 2008. The median and mode cloud-base heights were 685 and 670 mb, respectively. The selection of 670 mb as the prototypical cloud-base height over the southern plains was affirmed by the majority of convective cloud-base heights observed between 670 and 700 mb, and the availability of the 670-mb level as a pressure level for the temperature and dewpoint calculation from the GOES sounding retrieval.

Pryor (2010) presented statistical analysis of a dataset built by comparing wind gust speeds recorded by Oklahoma Mesonet stations to calculated predictors for 35 downburst events that yielded results similar to those presented in Srivastava (1985). Correlation was computed between key parameters in the downburst process, including $|\Gamma|$, ΔDD between the 670- and 850-mb levels, surface-based CAPE, and NEXRAD base reflectivity factor Z_h (0.5° elevation). The first important finding, as discussed in Pryor (2010), is a negative correlation ($r = -0.34$) between lapse rate and radar reflectivity factor with a confidence level above 99%. Other results in Pryor (2010) compare well with the findings in Srivastava (1985), where, for lapse rates greater than 8°C km^{-1}, downburst occurrence is nearly independent of radar reflectivity factor. For lapse rates less than 8°C km^{-1}, downburst occurrence was associated with high reflectivity factor (>50 dBZ) storms. The majority of downbursts occurred in subcloud environments with lapse rates greater than 8.5°C km^{-1}. Adding the dewpoint depression difference to the lapse rate yielded an even greater negative correlation ($r = -0.42$) when compared to the radar reflectivity factor. Finally, comparing the quantity $\Gamma + \Delta$DD to CAPE resulted in the strongest negative correlation ($r = -0.82$), with a confidence level again above 99%. This emphasizes the complementary nature of the $\Gamma + \Delta$DD and CAPE parameters as predictor variables.

2. Methodology

a. Microburst index formulation

The Microburst Windspeed Potential Index (MWPI; Pryor 2010, 2012, 2014), as compared to the WMSI defined in Table 1, is designed to quantify the most relevant factors in convective downburst generation in intermediate thermodynamic environments by incorporating 1) surface-based CAPE, 2) the temperature lapse rate between the 670- and 850-mb levels, and 3) ΔDD between the 670- and 850-mb levels. The MWPI is incorporated into a predictive linear model developed in the manner exemplified in Caracena and Flueck (1988). The MWPI formula consists of a set of predictor variables (i.e., dewpoint depression and temperature lapse rate) that generates output of the expected microburst risk. Analysis of microbursts during the JAWS project (Wakimoto 1985; Caracena and Flueck 1988) identified the following favorable environmental characteristics for high plains dry microbursts: 1) low surface dewpoint temperatures, 2) high convective cloud base, 3) small midtropospheric dewpoint temperature

[2] Temperature lapse rate refers to the negative vertical gradient in ambient temperature.

depression, and 4) high subcloud lapse rate. Consideration of 50 downburst events over Oklahoma and Texas during the summer of 2009 revealed that for the majority of downburst events, CAPE was greater than 1000 J kg^{-1} and ΔDD was greater than 5°C. Srivastava (1987) also noted that a minimum lapse rate of 5°C km^{-1}, associated with heavy precipitation and a high reflectivity factor (>50 dBZ), was necessary for intense downdraft generation. Thus, the scaling factors of 1000 J kg^{-1}, 5°C km^{-1}, and 5°C, respectively, are applied to the MWPI algorithm to yield a unitless MWPI value that expresses wind gust potential on a scale from 1 to 5:

$$\mathrm{MWPI} \equiv (\mathrm{CAPE}/1000\,\mathrm{J\,kg^{-1}}) + \{\Gamma/5^{\circ}\mathrm{C\,km^{-1}} + [(T - T_d)_{850} - (T - T_d)_{670}]/5^{\circ}\mathrm{C}\}. \quad (1)$$

The MWPI algorithm is expected to be most effective in assessing downburst wind gust potential associated with ordinary cell and multicell convective storms in weak wind shear environments.

Generation of the MWPI product is based on the following assumptions: 1) mixed-phase precipitation, in the form of snow, graupel, hail, and supercooled rain, is present in the middle level of the storm; 2) phase-change cooling (sublimation, melting, and evaporation) below the melting level is the primary forcing factor in negative buoyancy generation and the subsequent acceleration of convective storm downdrafts; 3) precipitation loading is a secondary forcing mechanism; and 4) the melting level is located at or above the 670-mb level (typically near the 3.5 km MSL altitude). Derivation of the MWPI algorithm is primarily based on parameter evaluation and pattern recognition techniques as employed in the severe convective storm forecasting process (Johns and Doswell 1992). Although the MWPI algorithm was originally designed for convective wind speed potential assessment in intermediate thermodynamic environments over the central United States, MWPI has demonstrated effectiveness for wet microbursts that occur over the eastern United States. For wet microburst environments, large CAPE and conditionally unstable temperature lapse rates (5–10°C km^{-1}) between the 670- and 850-mb levels would be readily detected by the MWPI algorithm. In addition, for 55 downburst events documented in the mid-Atlantic coastal region during the summers of 2010–13, a mean melting level height (ML) of 590 mb was found with a range of 560–630 mb. Thus, over the mid-Atlantic region, the 670–850-mb layer often coincides with the melting layer, and encompasses the region where downdraft acceleration due to the melting of ice-phase precipitation is expected to be at a maximum (Srivastava 1987). Intense hail-producing convective storms that develop in environments with large CAPE and an elevated melting level near or above the 670-mb level occur frequently during the warm season over the central and eastern United States. The assumption of the presence of ice-phase precipitation, especially in the form of hail, and its subsequent melting in the lower troposphere renders the MWPI a more effective warm-season prediction tool.

b. *Validation process*

The main objective of the validation effort is to quantitatively assess the performance of the MWPI algorithm by employing classical statistical analysis of real-time data as outlined in Pryor (2014). Accordingly, this effort entails a study of downburst events in a manner that emulates historic field projects such as the 1982 JAWS (Wakimoto 1985) and the 1986 Microburst and Severe Thunderstorm (MIST) project (Atkins and Wakimoto 1991). Algorithm output data were collected for downburst events that occurred during the warm season (especially between 1 June and 30 September) and were validated against surface observations of convective wind gusts as recorded by wind sensors in high quality mesonetworks, such as the Oklahoma and West Texas Mesonets (Brock et al. 1995; Schroeder et al. 2005), and over the Chesapeake Bay region by NOAA and WeatherFlow marine network stations. Figure 1 shows that the Oklahoma–Texas region, with an area of $\sim 4 \times 10^5$ km^2, is about 10 times larger than the Chesapeake Bay region that is sampled for this validation study. Note the high density of severe wind reports over the Maryland portion of the Chesapeake Bay watershed between 1955 and 2013. The importance of the choice of these geographic regions for product validation is discussed in more detail in section 3. The 10-km spacing of GOES sounding retrievals and resulting microburst risk algorithm output in clear-sky regions plotted over a visible or infrared GOES image facilitates the collocation of index values and measured downburst-related wind speeds at the surface. Wakimoto (1985) and Atkins and Wakimoto (1991) discussed the effectiveness of using mesonetwork surface observations and the radar reflectivity factor in the verification of the occurrence of downbursts. Site characteristics, data quality assurance, and wind sensor calibration are thoroughly documented in Brock et al. (1995) and Schroeder et al. (2005). Well-defined peaks in wind speed as well as significant temperature decreases (Wakimoto 1985; Atkins and Wakimoto 1991) were effective indicators of high reflectivity factor downburst occurrence.

As illustrated in the flowchart in Fig. 2, real-time experimental MWPI product images are generated by Man computer Interactive Data Access System (e.g., McIDAS-X). This program reads and processes GOES

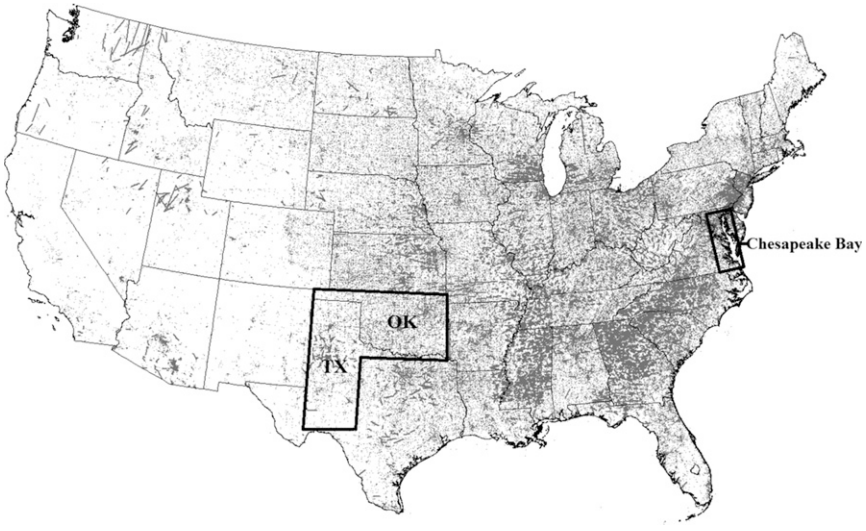

FIG. 1. Geographic regions of interest within the CONUS for the validation of the MWPI algorithm. Locations of all severe wind reports from the NOAA/Storm Prediction Center database between 1955 and 2013 are plotted over the image. (Courtesy of the NOAA/Storm Prediction Center. Available online at http://www.spc.noaa.gov/gis/svrgis/.)

sounder data, calculates and collates microburst risk values, and overlays risk values onto GOES imagery. Output images are then archived via FTP and Hypertext Transfer Protocol (HTTP) to the GOES Microburst Products web page. For selected downburst events, and for the case studies presented in this paper, MWPI product imagery, radar imagery, and thermodynamic diagrams were generated using McIDAS-V (available online at http://www.ssec.wisc.edu/mcidas/software/v/). The MWPI algorithm, as visualized by McIDAS-V, reads and processes GOES sounder data in binary format available on the GOES sounding profile web page (http://www.star.nesdis.noaa.gov/smcd/opdb/goes/soundings/html/sndbinary23L.html).

The MWPI is then calculated for each retrieval location and plotted on a user-defined map with a built-in McIDAS-V state projection for satellite imagery and a radar projection for radar reflectivity factor imagery. In addition, MWPI gridded fields and resulting contours as displayed on radar and satellite imagery are generated by McIDAS-V using the Barnes objective analysis (Barnes 1994a–c). Since sounding thermodynamic profiles in binary file format were archived for downburst events that occurred during and after the 2010 convective season, the scaling factors described in section 1 ($1000\,\mathrm{J\,kg^{-1}}$, $5^{\circ}\mathrm{C\,km^{-1}}$, and 5°C) were only applied to the calculation of MWPI values over the Chesapeake Bay region.

The Next Generation Weather Radar (NEXRAD) level-II Z_h and differential reflectivity factor Z_{DR} and Terminal Doppler Weather Radar (TDWR) Z_h were obtained from the National Climatic Data Center (NCDC) and used to verify that observed wind gusts were associated with downbursts originating from high reflectivity factor storms and were not associated with other types of convective wind phenomena (i.e., gust fronts). Plan-view images of the radar reflectivity factor Z were constructed from 0.5°-elevation angle scans. Equations (7.13) and (4.26) in Battan (1973) establish direct proportionality between liquid water content M and effective reflectivity factor Z_e. An additional application of radar reflectivity factor imagery is to infer microscale physical properties of downburst-producing convective storms. Differential reflectivity factor was employed in the case studies in this paper to analyze the vertical precipitation composition in convective storms and thereby indicate the presence of hail and discuss its role in the enhancement of convective downdrafts. Particular reflectivity factor signatures, such as the spearhead echo (Fujita and Byers 1977), bow echo (Fujita 1978; Przybylinski 1995), and protrusion echo (Knupp 1996), are effective indicators of the occurrence of downbursts and were employed in this study to indicate downburst occurrence.

Since surface data quality is paramount in an effective validation program, relatively flat, sparsely forested prairie regions were initially chosen as study regions. The mostly treeless, low-relief topography that dominates sparsely populated regions such as the high plains in the United States allowed for the assumption of horizontal homogeneity when deriving a conceptual model of a boundary layer thermodynamic structure favorable for

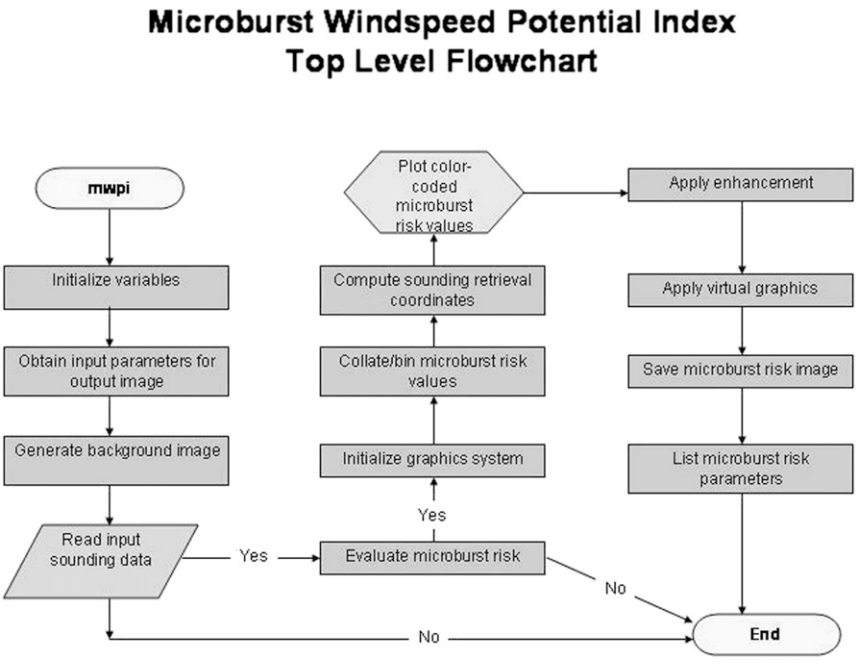

FIG. 2. Flowchart illustrating the operation of the MWPI program in the McIDAS-X environment.

downbursts. More importantly, planar topography and water body surfaces facilitate relatively smooth flow (due to small surface roughness) with respect to downburst winds in which drag and turbulent eddy circulation resulting from surface obstructions (i.e., buildings, hills, and trees) are minimized. Sorbjan (1989) describes the wind profile in the surface layer and dictates that the relatively small roughness parameter of shortgrass prairie would permit wind gust measurements that are more representative of downburst intensity. Over the eastern United States, Atlantic coastal waters are optimal for a validation study. Observational data from the National Data Buoy Center (NDBC; http://www.ndbc.noaa.gov/) and WeatherFlow (http://datascope.weatherflow.com/) was preferred for algorithm validation.

Doswell and Schultz (2006) stated that time-lag correlation between a candidate forecast parameter and verifying observations is important in quantitatively establishing forecast accuracy as a function of lead time. Accordingly, for this study, in order to assess the predictive value of the MWPI and $\Delta\theta_e$ algorithm output, the closest representative index values were obtained for retrieval times 1–3 hours prior to the observed surface wind gusts. Representativeness of proximate index values was inferred by analysis of surface observations, radar, and satellite imagery so that no appreciable change in environmental static stability and airmass characteristics between product valid time and time of observed downbursts had occurred. Furthermore, in order for the downburst observation to be included in a validation dataset, it was required that the parent convective storm cell of each downburst, with a radar reflectivity factor greater than 35 dBZ, be located nearly overhead at the time of downburst occurrence. Srivastava (1987), for the purpose of a modeling study, arbitrarily selected 20 m s^{-1} [40 knots (kt; where 1 kt = 0.51 m s^{-1})] as the minimum downdraft intensity (vertical velocity) associated with a downburst, and compared model results to JAWS observations to derive a physical mechanism for wet downbursts. Similarly, the model in Fig. 10 and Eq. (2) of Wakimoto (1985) was applied to five downburst events during the JAWS project to calculate near-surface vertical velocities associated with each downburst. The calculated vertical velocities were directly compared to observed peak horizontal wind speeds associated with each downburst event and documented in Table 3 of Wakimoto (1985), where it was noted that for each downburst, vertical velocities were of the same magnitude as horizontal wind speeds. The current study includes marginal convective wind events with horizontal peak wind speed observations of at least 18 m s^{-1} (34 kt) or greater. A technique devised by Wakimoto (1985) to visually inspect horizontal wind speed observations over the time intervals encompassing candidate downburst events was implemented to exclude gust front events from the validation dataset. In summary, the screening process employed to build the validation dataset that consists of criteria based on surface weather observations

TABLE 2. MWPI validation statistics based on direct comparison between index values and measured downburst wind gusts. In the regression line equations, x represents the MWPI value while y represents the predicted wind gust speed.

	Oklahoma–Texas MWPI ($N = 208$)	Mid-Atlantic MWPI ($N = 55$)	Mid-Atlantic $\Delta\theta_e$ ($N = 55$)
MAE (kt)	−0.55	0.03	—
Correlation	0.62	0.62	0.39
t value	9.23	45.5	11.75
Critical value ($P < 0.0005$)	3.34	3.48	3.48
Confidence level (%)	>99.95	>99.95	>99.95
Regression line equation	$y = 0.3163x + 33.766$	$y = 3.775x + 29.9639$	—

and the radar reflectivity factor yielded a sample size of downbursts and associated index values adequately large enough to determine the confidence level of the validation results.

Similar to previously developed GOES-derived microburst products, wind gust potential expressed in the MWPI is conditional on the occurrence of convective storms and is not intended to be a stand-alone predictor, but, is more effectively used as a supplement to other data sources such as NEXRAD reflectivity factor. In accordance with Ellrod et al. (2000), validation metrics such as probability of detection (POD) and false alarm ratio (FAR) were not considered to be representative of the performance of the MWPI in this study. Thus, the covariance and mean difference between the variables of interest, MWPI and surface downburst wind gust speed, were analyzed. Algorithm effectiveness was assessed as the correlation between MWPI values and observed surface wind gust velocities, as well as the mean absolute error (MAE) between MWPI-predicted downburst wind gust speeds (based on the linear regression equations noted in Table 2) and observed surface wind gust speeds resulting from downbursts. Statistical significance testing, specifically, a Student's t test for correlated samples (Lowry 2014), was conducted, in the manner outlined in Pryor and Ellrod (2004a,b), to determine the confidence level of the correlation between observed downburst wind gust magnitude and microburst risk values. Examples of MWPI algorithm validation employing the direct comparison method are shown graphically in the case studies in section 4. MWPI values are not expressed in dimensions of wind speed, but are related to wind speed through the regression line equations presented in Table 2.

3. Validation results

Validation of the MWPI product was conducted for the summer season (between 1 June and 30 September) for two distinct regions of the continental United States: the southern Great Plains region between 2007 and 2010 and the mid-Atlantic coastal region between 2010 and 2013. Table 2 outlines the results of validation statistical analysis over these two distinct climatic regions: the southern Great Plains region varies from semiarid to humid from west to east, while the mid-Atlantic region is entirely humid. The mean absolute error represents the average difference between the MWPI-derived predicted wind gust speed y, based on regression line equations for each region, and the observed downburst-related wind gust speed.

Over the southern plains region, GOES sounder–derived MWPI values were directly compared to Mesonet observations of downburst winds over Oklahoma and Texas for 208 events between June 2007 and September 2010. The correlation between MWPI values and measured wind gusts was $r = 0.62$ with a confidence level near 100%, indicating that the likelihood of this correlation resulting from chance or random variability is very small (less than 0.1%). Pryor (2012) outlined the results of the comparison of MWPI values to measured downburst-related wind gust speeds that identified two clusters of data points that correspond to observed wind gusts between 18 and 26 $m\,s^{-1}$ (35–50 kt) and observed wind gusts greater than 26 $m\,s^{-1}$ (50 kt). The MAE of −0.55 shows a slight tendency of the MWPI to underestimate wind gust potential over the southern plains region. This region, as identified by Schaefer et al. (2004), is characterized as a maximum in the frequency of large hail. The following case studies will highlight the importance of frozen precipitation, especially hail, and in forcing and sustaining downdraft acceleration.

Within the mid-Atlantic coastal region, the Chesapeake Bay area was the region of focus for the microburst product validation. A recent study by Smith et al. (2013), based on 1911 severe thunderstorm wind gusts measured by automated weather observing stations in the contiguous United States between 2003 and 2009, identified that the Maryland portion of the Chesapeake Bay watershed was located within a region with an elevated frequency of severe thunderstorm wind occurrence. The majority of severe wind gusts observed in this region originated from quasi-linear convective systems or disorganized storms. In addition, a dense marine weather

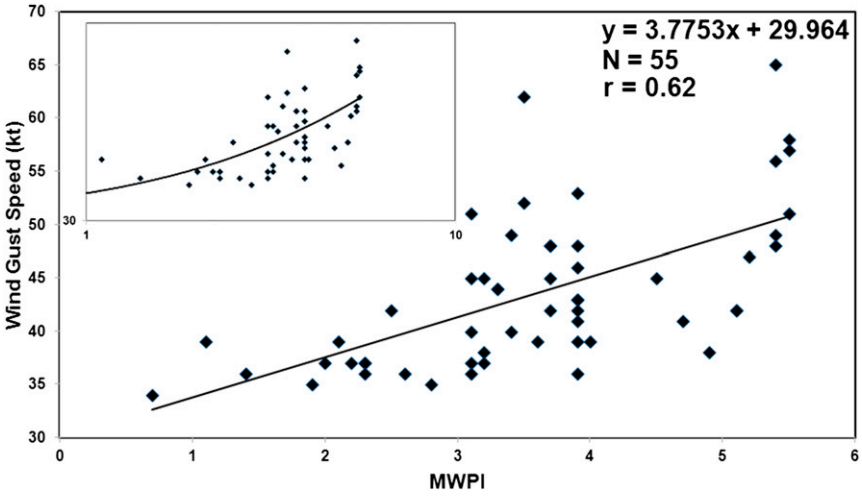

FIG. 3. Scatterplot of MWPI values vs measured downburst-related wind gust speeds (kt) for 55 events over the Chesapeake Bay region between 2010 and 2013. Inset shows the $\log_{10}$ transformation of the scatter diagram with the resulting regression curve.

observing network including NOAA tower-mounted stations and weather data buoys that exists over the Chesapeake Bay and adjacent estuaries allowed for frequent sampling of downburst-related winds. Direct comparison between MWPI values and observed wind gusts from the period of summer 2010 to summer 2013 yielded a data sample of 55 recorded downburst wind events. Applying the scaling factors described in section 2, correlation between MWPI values was also found to be 0.62. This result is described graphically by the scatter diagram in Fig. 3, where increasing deviation from the regression line (or variance) with increasing MWPI is evident. Although a small MAE of 0.02 m s^{-1} (0.03 kt) was found over the Chesapeake Bay region, the number of outliers in the scatterplot in Fig. 3 increases with increasing MWPI value. In consideration of the factors that result in a larger deviation from the regression line, a logarithmic transformation ($\log_{10}$) was applied to both axes of the scatter diagram in Fig. 3, with the result shown in the inset. The resulting log–log model shows a better fit of the regression curve to the variance in the data points, and suggests an effective logarithmic relationship between MWPI and downburst-related wind gust speed.

4. Case studies

a. Maryland Chesapeake Bay downbursts

During the afternoon of 10 July 2013, multicellular convective storms developed and moved eastward over the piedmont region of central and southern Virginia. These multicell storms evolved in a warm, moist, and generally unstable air mass well ahead of a cold front moving through the Ohio River valley region. A small mesoscale convective system (MCS) that tracked through central Virginia during late afternoon generated a cold pool that moved downshear (northeastward) toward northern Virginia and southern Maryland. By early evening (2300 UTC), the downshear cold-pool boundary moved into a very moist and convectively unstable region with observed surface dewpoints greater than 23°C. Enhanced convergence and resultant lifting along the boundary triggered the development of new multicellular storms over northern Virginia and southern Maryland in the vicinity of the Potomac River. Figure 4 shows a regional view of *GOES-13* sounder–derived MWPI values between 2045 and 2145 UTC. Note a maximum in MWPI values over the central and lower Chesapeake Bay and a general decrease in MWPI values northward over the upper Chesapeake Bay and westward toward the Washington, D.C., metropolitan area. Application of the mid-Atlantic region linear regression equation as presented in Table 2 to MWPI values of 3–5 that were the closest representative values over the central Chesapeake Bay region yielded wind gust potential of 22–25 m s^{-1} (42–48 kt) over 3 h prior to downburst wind occurrence. In a similar manner, an MWPI value of 2.3 near the upper Chesapeake Bay was associated with wind gust potential near 19 m s^{-1} (37 kt). Figure 5, the Sterling, Virginia, radiosonde observation (raob) thermodynamic profile at 0000 UTC, graphically describes attributes of the preconvective environment that indicated potential for intense storm downdrafts and resulting strong downburst winds. Of interest is a layer in the lower to midtroposphere, between the 680- and 780-mb levels, with a conditionally unstable temperature lapse rate (6.5°C km^{-1}), increasing dewpoint depression with

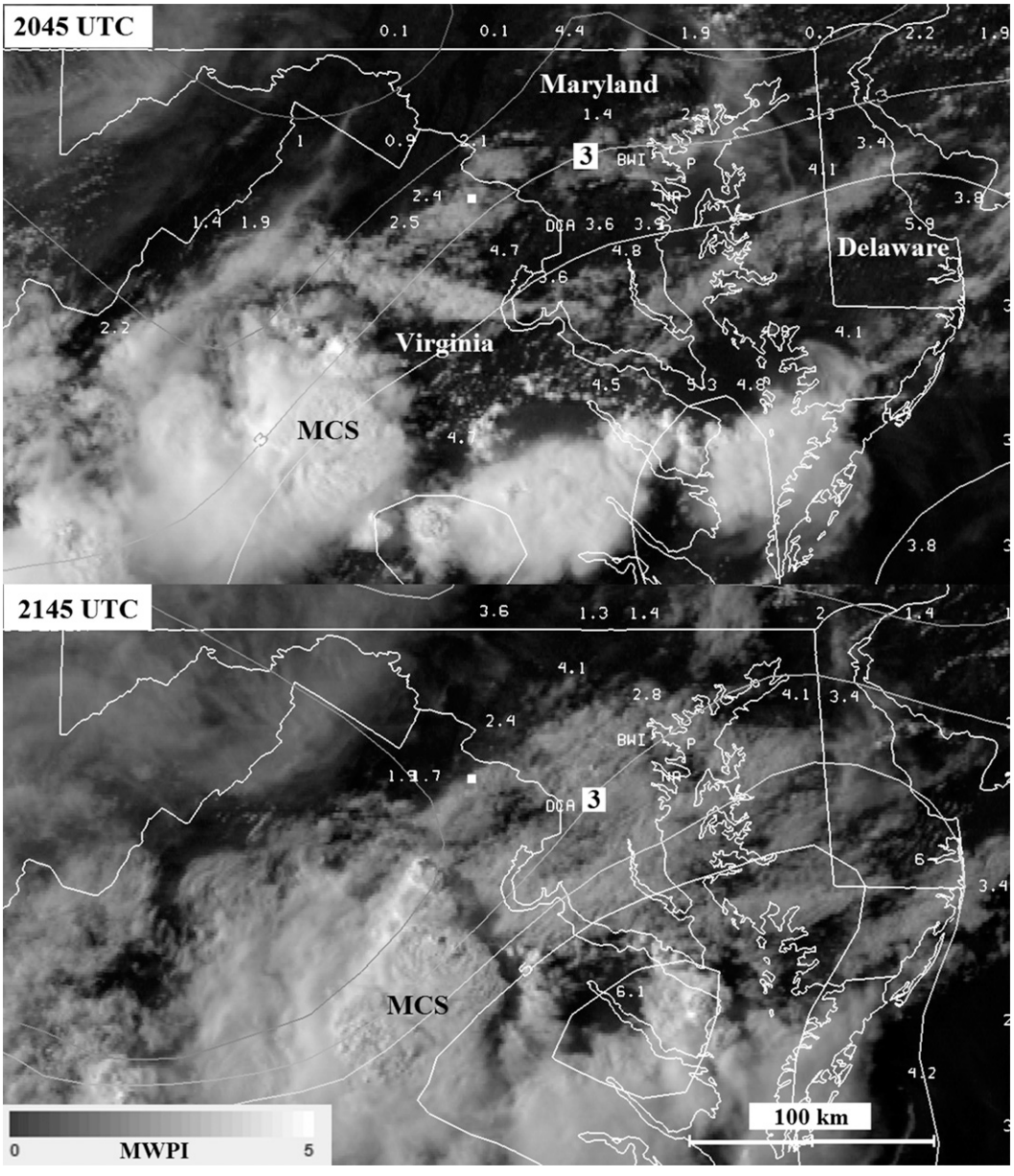

FIG. 4. *GOES-13* MWPI images over the mid-Atlantic region with an McIDAS-V Maryland projection at (top) 2045 and (bottom) 2145 UTC 10 Jul 2013. Contours of grid-interpolated MWPI values overlie MWPI values plotted at sounding retrieval locations and *GOES-13* visible imagery. The contour interval is 1 and the contour for an MWPI value of 3 is labeled. The filled white square marks the location of the Sterling raob site. DCA, Baltimore–Washington International Airport (BWI), the U.S. Naval Academy at Annapolis METAR station (NA), and the Patapsco buoy (P) are marked.

decreasing height above ground level, and a virtual temperature excess of around 3°C over absolute temperature in the boundary layer. Srivastava (1987) found a vertical velocity of 20 m s^{-1} or greater can be generated by a convective storm with a radar reflectivity factor of greater than 50 dBZ near the melting level and an environmental lapse rate of 6°C km^{-1} or greater below the melting level. The MWPI value calculated from this thermodynamic profile was 3.9, corresponding to peak horizontal wind speed potential near 23 m s^{-1} (45 kt) and supported the ability of the MWPI algorithm to detect a statically unstable environment that was expressed as elevated index values with downburst wind gust potential greater than 20 m s^{-1} (40 kt).

During the early evening, between 2300 UTC 10 July and 0000 UTC 11 July 2013, two particularly intense

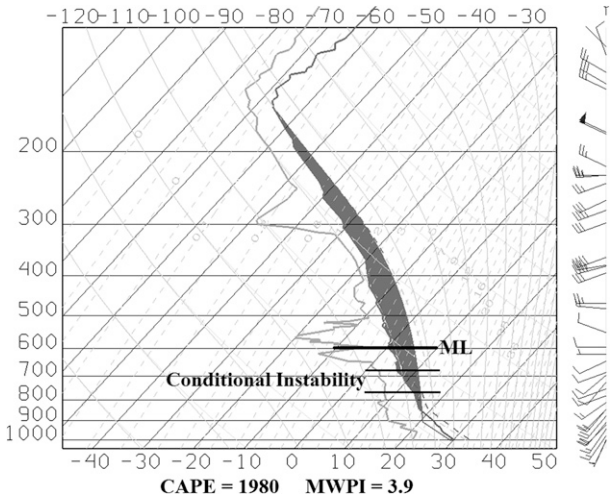

FIG. 5. Raob sounding thermodynamic profile over Sterling at 0000 UTC 11 Jul 2013. The dashed curve represents virtual temperature. The ML (0°C isotherm) is indicated. Mean layer CAPE ($J\,kg^{-1}$) is represented by the shaded area. The vertical axis is labeled in units of pressure (mb) and the horizontal axis is labeled in units of temperature (°C).

multicell storms developed and tracked northeastward toward the metropolitan area of Washington, D.C., and the Maryland Chesapeake Bay western shore. As shown in Fig. 6, the storm that would eventually produce a weak downburst at Ronald Reagan Washington National Airport (DCA) evolved from the merging of a broken line of ordinary cell storms between 2330 and 0000 UTC. During this same time period, a multicell storm evolved from an ordinary cell that moved from southern Maryland to the western shore of the Chesapeake Bay. Both multicell storms indicated a preferred tendency for new cell development on the northern flank, while moving northeastward. Figure 6 also illustrates the evolution of the multicell storm just prior to downburst occurrence over DCA. This storm was dominated by a high reflectivity factor (>50 dBZ) and well-defined protrusion echoes on its forward flank. Near the time of downburst occurrence at 0004 UTC, a new, small protrusion echo was apparent over DCA. Although a gust potential of $22\,m\,s^{-1}$ (43 kt) was indicated by a proximate MWPI value of 3.6, the observed peak wind gust associated with the downburst that occurred at DCA was only $18\,m\,s^{-1}$ (34 kt).

After downburst occurrence in the area of Washington, D.C., the western shore multicell storm rapidly intensified while approaching the area of Annapolis, Maryland. Figure 7 shows that two protrusion echoes were becoming apparent on the northeastern (forward) flank of the storm by 0023 UTC, as the maximum base reflectivity factor was exceeding 50 dBZ. These protrusion echoes continued to evolve downwind until the commencement of downburst winds over the Annapolis harbor at 0028 UTC. By 0033 UTC, wind observations from the Greenbury Point WeatherFlow Station and NOAA's Annapolis buoy, documented in Table 3, indicated surface wind divergence associated with downburst occurrence as the precipitation core of the storm passed nearly overhead. Figures 8 and 9 show corresponding base reflectivity factor and differential reflectivity factor range–height indicator (RHI) transects for downburst-producing storms at Washington, D.C., and over Annapolis harbor, respectively. Recorded downburst-related wind gusts in the Annapolis harbor of $22–25\,m\,s^{-1}$ (42–48 kt), between 0028 and 0033 UTC, originated from an intense cell on the leading edge of the multicell storm. The Z_h RHI transect at 0029 UTC indicated a taller and more intense convective storm cell compared to the storm in Washington, D.C., with a concentrated high reflectivity factor core over the Annapolis harbor near the time of downburst occurrence. Likewise, the corresponding Z_{DR} RHI transect at 0029 UTC, compared with the earlier transect at 0004 UTC, shows a likelihood that the stronger downburst-producing storm over Annapolis had a core of graupel and hail immediately below the melting level, with a shaft of heavy rain dominated by large drops extending from below the melting level toward the surface. The transect displayed that over the location of downburst occurrence [the NDBC Annapolis buoy (AN)], Z_{DR} values between −1 and +1 dBZ, extending from the melting level downward to about 3 km above ground level, were nearly collocated with reflectivity factor values greater than 50 dBZ. This condition, as noted by Bringi and Chandrasekar (2001) for a hailstorm over Germany and Brandes and Ryzhkov (2004) for an Oklahoma hailstorm, strongly indicated the presence of hail and favored stronger downburst wind gusts over the Annapolis harbor than that recorded at Washington, D.C., about 30 min earlier. The loading of graupel and hail in the Annapolis storm was likely a factor in the enhancement of downdraft intensity. In the manner exemplified by Srivastava (1987), the generation of larger negative buoyancy resulting from the combined effects of sublimation and melting of falling hail, as well as the subsequent evaporation of rain produced by hail melting, increased the downdraft velocity.

After 0030 UTC, the multicell storm continued to track northward over the upper Chesapeake Bay and into a slightly more stable environment, as indicated by MWPI values between 2 and 3. Between 0050 and 0100 UTC, the NOAA Patapsco buoy near Baltimore recorded a weaker downburst wind gust of $19\,m\,s^{-1}$ (38 kt): very close to the value predicted by the MWPI formula. Based on this data sample, a correlation between MWPI values and measured wind gusts of 0.54

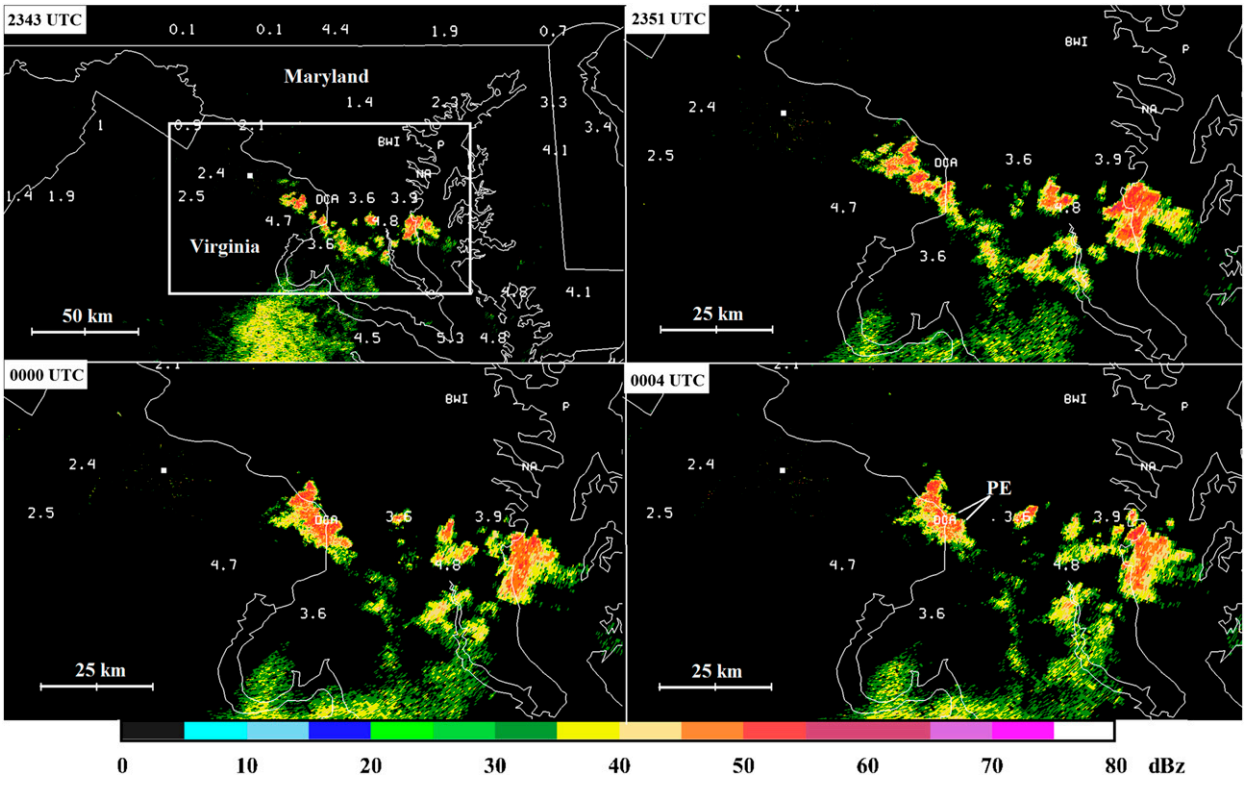

FIG. 6. Sterling NEXRAD Z_h (dBZ) at (top left) 2343 and (top right) 2351 UTC 10 Jul 2013 and at (bottom left) 0000 and (bottom right) 0004 UTC 11 Jul 2013. *GOES-13* MWPI values at 2045 UTC are plotted over the images. The white rectangle (top left) shows the domain of the images between 2351 and 0004 UTC. The location of protrusion echoes (PE) is indicated (bottom right).

was found for this downburst event. Excluding the weaker downburst event observed at Washington, D.C., the correlation increased to 0.74. Despite the overestimation in wind gust potential at Washington, D.C., this case demonstrated the capability of the GOES MWPI product to effectively indicate gust potential with a significantly longer lead time as compared to the use of only Doppler radar imagery.

b. *Northeastern Florida downbursts*

Sea-breeze fronts that develop along the Gulf of Mexico and Atlantic coastal regions, as well as the interaction between these fronts at the sea-breeze convergence zone over the Florida Peninsula, frequently serve as an initiating mechanism for deep convective storms that produce downburst activity. A confirmed downburst event on 10 June 2014 in Jacksonville, Florida, demonstrated an effective application of the mid-Atlantic MWPI predictive model. During the afternoon of 10 June, clusters of strong thunderstorms developed along the Atlantic coast sea-breeze front in east-central Florida and then moved northward toward the Jacksonville area. Outflow boundary interaction with the sea-breeze front and the subsequent merger of a cluster of thunderstorms over the western portion of Jacksonville during the late afternoon resulted in the development of a large, high reflectivity factor thunderstorm that would eventually produce a strong downburst at Whitehouse Naval Outlying Field.

Figure 10 shows the evolution of convective cloud systems and the thermodynamic environment during the 3-h period prior to the downburst at Whitehouse Naval Outlying Field. MWPI values of 3 or greater, indicating downburst wind gust potential of 20 m s^{-1} (40 kt) or greater, persisted over northeastern Florida near the sea-breeze front through the afternoon. During the period of 1800–2100 UTC, two bands of enhanced cumulus clouds merged over Jacksonville while intense deep convection that developed over east-central Florida was spreading northward. Application of the linear regression technique to MWPI values of 2.8–3.6 over Jacksonville yielded wind gust potential of 20–22 m s^{-1} (40–44 kt) nearly 2 h prior to downburst wind occurrence at Whitehouse Naval Outlying Field. Figure 11, a thermodynamic profile generated from a Rapid Refresh (RAP) model analysis at 2000 UTC over Whitehouse Naval Outlying Field, displays the presence of large surface-based CAPE (>3000 J kg^{-1}) that signifies the

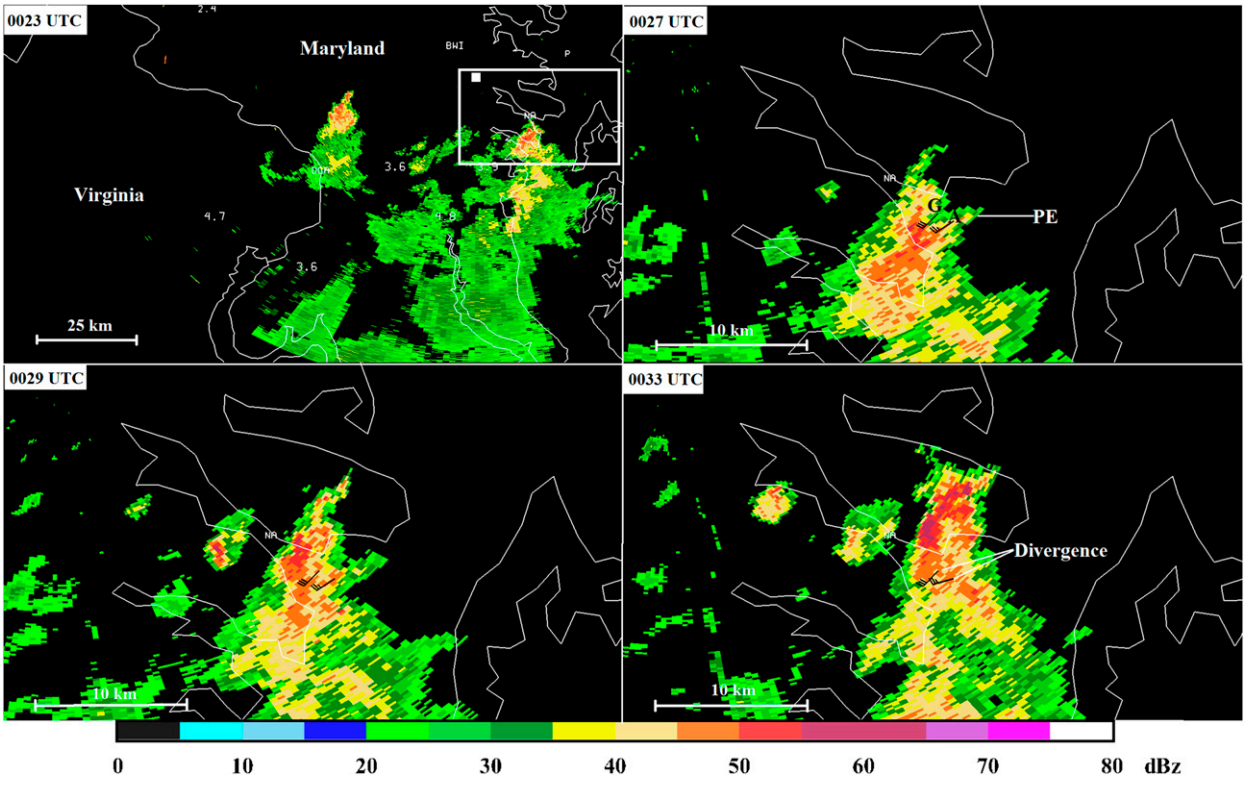

FIG. 7. BWI TDWR Z_h (dBZ) at (top left) 0023, (top right) 0027, (bottom left) 0029, and (bottom right) 0033 UTC 11 Jul 2013. The white rectangle (top left) shows the domain of the images between 0027 and 0033 UTC. The white filled square marks the location of the BWI TDWR. Greenbury Point WeatherFlow station (G), NOAA Annapolis buoy (A), and the PE are indicated (top right).

potential for storms with high precipitation content, especially in the form of graupel and hail. In addition, the thermodynamic profile indicated a 200-mb-deep layer of conditional instability below the melting level and a virtual temperature excess of around 3 K over absolute temperature in the boundary layer. Srivastava (1987) noted that all of these conditions contribute to strong downbursts with wind speeds of 20 m s^{-1} (40 kt) or greater.

By 2100 UTC, Jacksonville NEXRAD base reflectivity factor imagery in Fig. 12 displayed isolated, ordinary thunderstorm cell development over the western part of Jacksonville along the sea-breeze front while a large cluster of storms south of Jacksonville was expanding northward. The large thunderstorm cluster produced hail, measured at 2 cm (0.75 in.) near Orange Park at 2120 UTC, before merging with ordinary cell activity near Whitehouse Naval Outlying Field. Storm merging occurred over western Jacksonville between 2120 and 2140 UTC (not shown). Upon merging, the new thunderstorm evolved into a large, quasi-circular storm dominated by a high reflectivity factor (>50 dBZ) with an east–west dimension of 15 km. Between 2140 and 2151 UTC, Fig. 12 shows that several protrusion echoes became apparent, especially on the northern and eastern flanks of the storm. At 2150 UTC, a wind gust of 25 m s^{-1} (48 kt) was recorded at Whitehouse Naval Outlying Field and was confirmed as resulting from a downburst.

Radar imagery from the NEXRAD at nearby Moody Air Force Base, Georgia, was also employed for comparison to

TABLE 3. Measured wind gusts and associated microburst risk values for the 11 Jul 2013 Maryland Chesapeake Bay downburst event. WeatherFlow (WF) stations and NDBC buoys are indicated in the station column.

Station	Time (UTC)	Wind gust speed (kt)	$\Delta\theta_e$ (°C)	MWPI	MWPI WGP (kt)
Washington, D.C. (METAR)	0005	34	22	3.6	43
Tolly Point, Maryland (WF)	0022	39	21	3.9	45
Greenbury Point, Maryland (WF)	0033	48	21	3.9	45
Annapolis buoy, Maryland (NDBC)	0040	42	21	3.9	45
Patapsco buoy, Maryland (NDBC)	0100	38	24	2.3	38

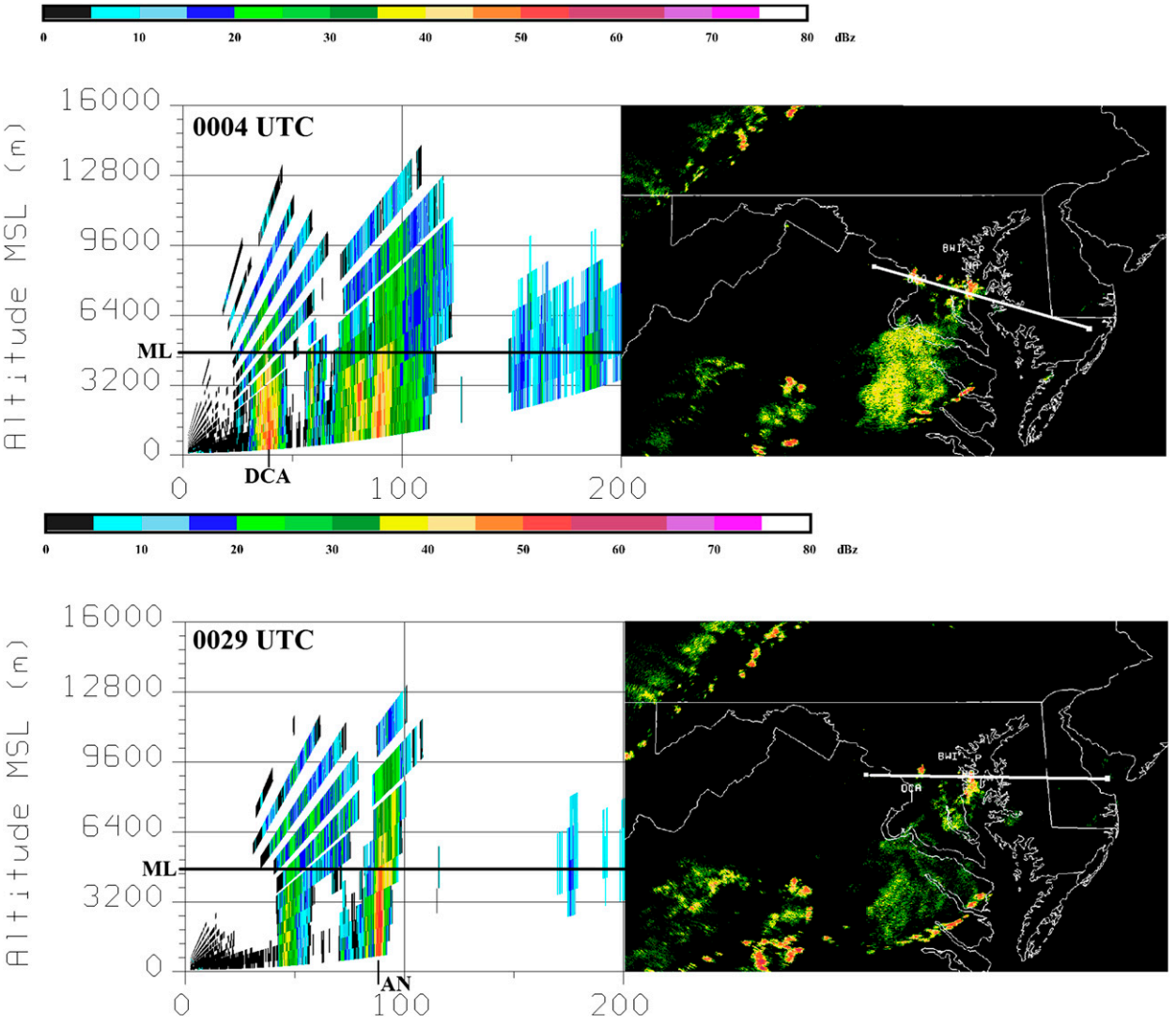

FIG. 8. Sterling WSR-88D Z_h (left) RHI and (right) PPI images at (top) 0004 and (bottom) 0029 UTC 11 Jul 2013. The white line segment in the PPI images shows a horizontal distance scale of the RHI transect of 200 km. DCA (top) and AN (bottom) mark the location of downburst occurrence. The ML from the thermodynamic profile shown in Fig. 5 is indicated (left).

patterns identified by Jacksonville NEXRAD imagery as well as to construct RHI images of the base reflectivity factor and differential reflectivity factor to analyze storm structure. The Moody Air Force Base NEXRAD base reflectivity factor image in Fig. 13 at 2142 UTC, just prior to downburst occurrence at Whitehouse Naval Outlying Field, shows a large high reflectivity factor storm over Jacksonville with several protrusions extending from the center of the storm. The base reflectivity factor RHI image reveals this storm to be a tall and wide echo with a reflectivity factor of 50 dBZ or greater extending upward to nearly 12 km above ground level. The corresponding Z_{DR} RHI transect shows that this strong downburst-producing storm most likely had a large core of graupel and hail near the melting level, with a shaft of heavy rain dominated by large drops extending from the melting level toward the surface. The transect displayed that over the location of downburst occurrence, Z_{DR} values between −1 and 0 dBZ were nearly collocated with reflectivity factor values greater than 50 dBZ. In addition, this measured downburst-related wind gust was recorded after a severe thunderstorm warning issued by the Jacksonville National Weather Service Forecast Office had expired at 2145 UTC. Later during the evening of 10 June, this thunderstorm cluster produced a weaker downburst wind gust of 21 m s^{-1} (41 kt) at Waycross–Ware County Airport, Georgia, where 1945 UTC MWPI values were somewhat lower, near 1.9.

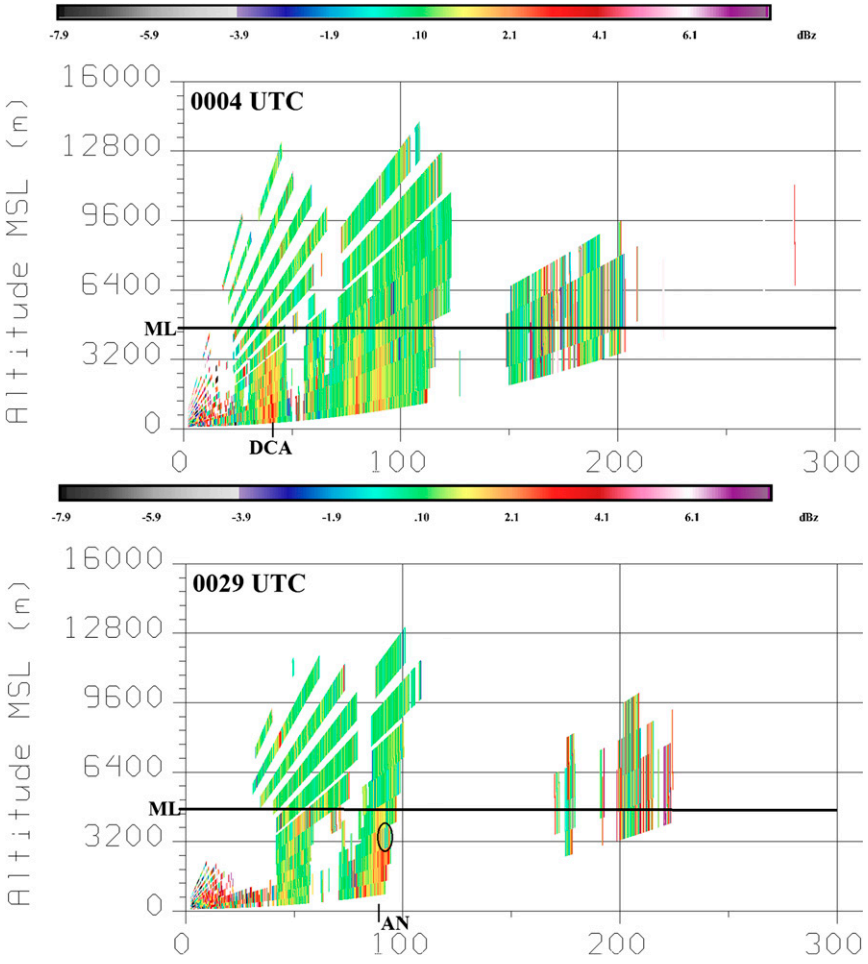

FIG. 9. Sterling WSR-88D Z_{DR} (dBZ) RHI images at (top) 0004 and (bottom) 0029 UTC 11 Jul 2013. The circled region (bottom) indicates the presence of graupel and hail immediately below the ML. DCA (top) and AN (bottom) mark the location of downburst occurrence. The ML from the thermodynamic profile shown in Fig. 5 is indicated. The distance scale is as shown in the corresponding PPI images in Fig. 8 (right).

5. Discussion

Pryor (2012) presents case studies of noteworthy downburst events that occurred over the southern Great Plains. The more recent case studies presented in this paper highlight the adaptability of the MWPI algorithm in more humid climatic and geographic regions in the continental United States, especially the Atlantic coastal region. These case studies highlight the flexibility of the MWPI prediction algorithm that can be refined or tuned based on regional climatology. The MWPI has demonstrated in these case studies the conditional capability to forecast, with up to 4-h lead time, thunderstorm-generated wind gusts that could present a hazard to marine and aviation transportation. In addition, the most intense downburst occurrence was found near local maxima in MWPI values, as highlighted in Figs. 4 and 10.

One apparent challenge in the application of the MWPI product over humid regions is the influence of precipitation phase and particle size distribution in a convective storm. The MWPI formula does not explicitly account for precipitation phase or particle size distribution and, thus, in some cases, will either overestimate or underestimate wind gust potential depending on the concentration and particle size distribution of ice-phase precipitation (Srivastava 1987). The Chesapeake Bay case demonstrated that convective storms with a core of graupel and hail near the melting level detectable by polarimetric Doppler radar show a tendency for stronger downbursts in which the resulting measured wind gust speeds are closer to the predicted value derived from the MWPI. A scenario for overestimation by the MWPI can be exemplified by the multicell storm that tracked over Washington, D.C., on 10 July 2013 and produced marginal downburst-generated

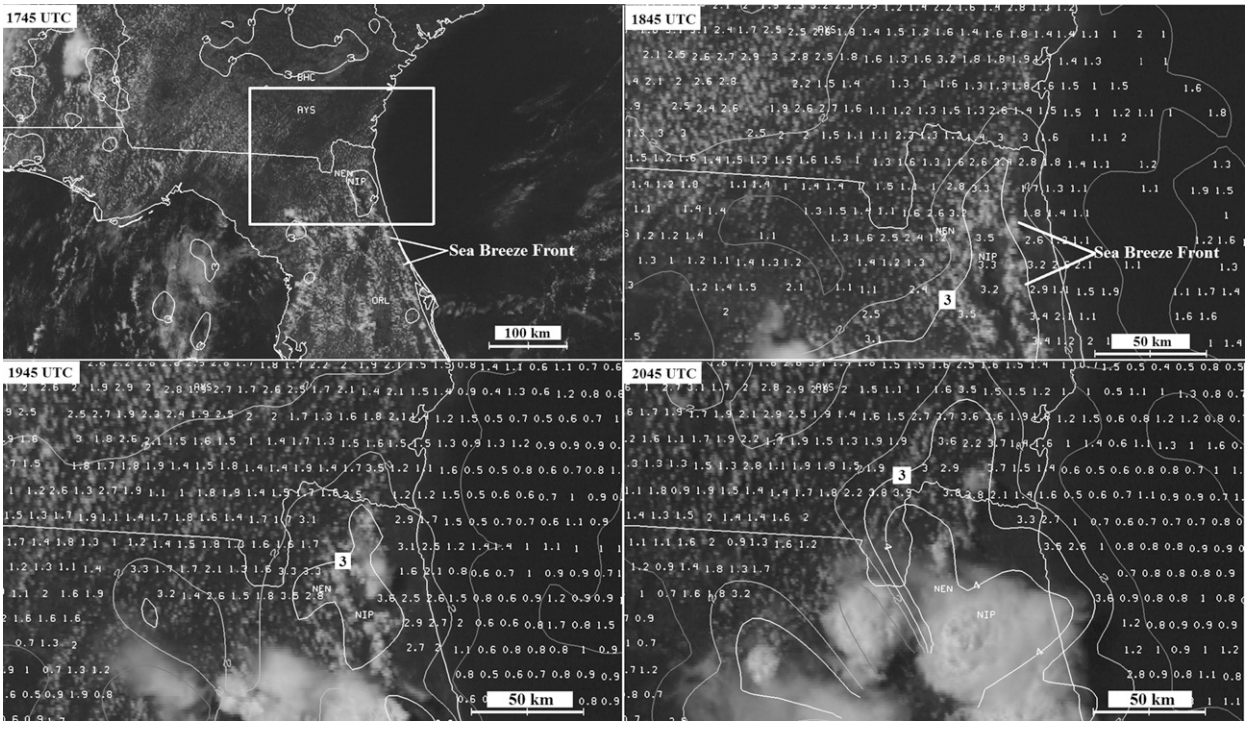

FIG. 10. *GOES-13* MWPI images at (top left) 1745, (top right) 1845, (bottom left) 1945, and (bottom right) 2045 UTC 10 Jun 2014. A white rectangle shows the domain of the images between 1845 and 2045 UTC, and a contour represents MWPI values greater than 3 (top left). In (top right), (bottom left), and (bottom right), contours of grid-interpolated MWPI values overlie MWPI values plotted at sounding retrieval locations. The contour interval is 1 and the contour for an MWPI value of 3 is labeled. Whitehouse Naval Outlying Field in Jacksonville (NEN), Jacksonville Naval Air Station (NIP), and airports at Waycross–Ware (AYS) and Baxley (BHC), Georgia, are indicated.

surface winds. This storm had no discernible compact region of low Z_{DR} near the melting level, although the storm was dominated by high Z_h. The MWPI overestimated the wind gust potential by nearly 5 m s^{-1} (10 kt) most likely because of the lack of graupel and hail in this storm. This result complements the finding of Srivastava (1987) that attributes stronger downburst wind speed to the presence of ice (especially hail) in midlatitude, warm-season convective storms. A scenario for MWPI underestimation would result from a convective storm with a precipitation core composed of a high concentration of smaller ice particles. Srivastava (1987) found that a particle size distribution consisting of a high concentration of smaller particles, both ice and liquid, further enhances downdraft intensity and noted that in the case of two storms with similar precipitation content, the storm with a higher concentration of smaller particles will produce a stronger downdraft.

The two uppermost outliers in the scattergram in Fig. 3 (32 and 34 m s^{-1} or 62 and 65 kt, respectively) are associated with downburst-related wind gusts that occurred over the lower Chesapeake Bay, Virginia, on 24 July 2012. The MWPI underestimated wind gust potential by 8–9 m s^{-1} (15–18 kt) during this event that consisted of a linear multicell storm, with bow echo characteristics, that tracked rapidly at 18 m s^{-1} (34 kt) from southeastern Virginia into the Atlantic Ocean. Analysis of the NEXRAD base and differential reflectivity factor (not shown) revealed patterns similar to those found in the Annapolis and Jacksonville downburst

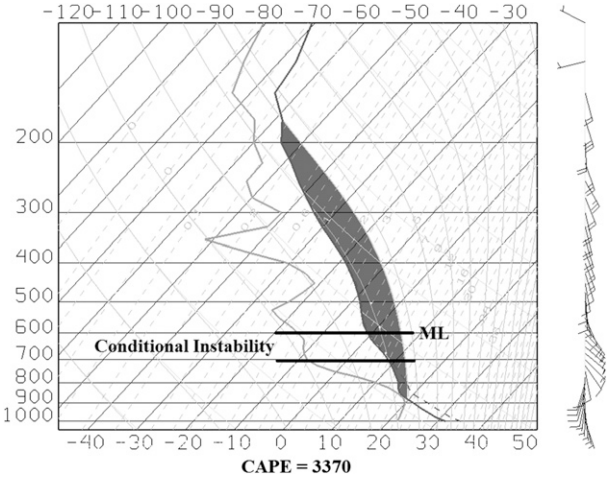

FIG. 11. RAP sounding thermodynamic profile over NEN at 2000 UTC 10 Jun 2014. The dashed curve represents virtual temperature, and ML (0°C isotherm) is indicated. Surface-based CAPE (J kg^{-1}) is represented by the shaded area. The vertical axis is labeled in units of pressure (mb) and the horizontal axis is labeled in units of temperature (°C).

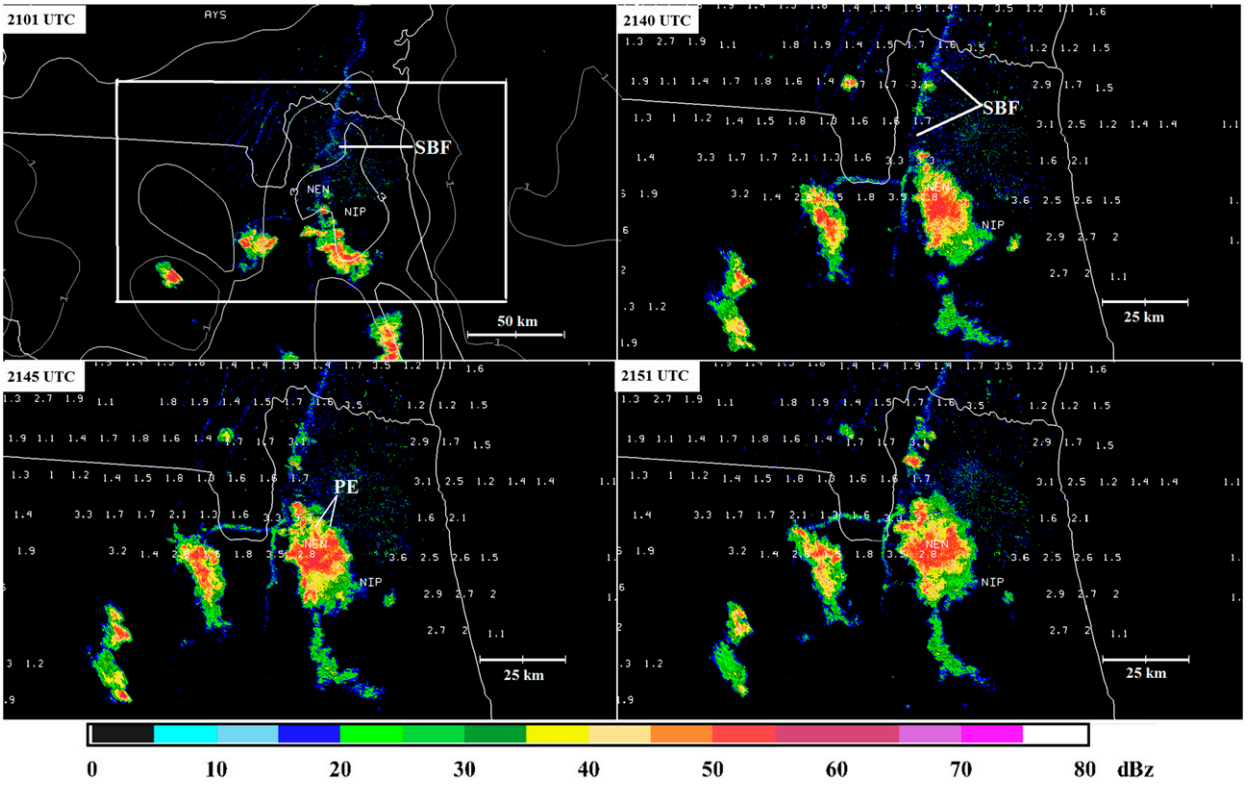

FIG. 12. Jacksonville NEXRAD Z_h (dBZ) at (top left) 2101, (top right) 2140, (bottom left) 2145, and (bottom right) 2151 UTC 10 Jun 2014. NEN, NIP, and AYS are labeled. The white rectangle (top left) shows the domain of the images between 2140 and 2151 UTC. The sea-breeze front (SBF; top left, top right) and PE (bottom left) are marked.

cases previously discussed. This thunderstorm complex likely had a core of graupel or small hail near the melting level just prior to downburst occurrence. In addition, analysis of NEXRAD radial velocity (not shown) indicated a low-level wind speed maximum ($>30\,\mathrm{m\,s^{-1}}$ or 60 kt), likely associated with a descending rear-inflow jet (Weisman 1992), in proximity to the location of measured peak horizontal wind speeds ($34\,\mathrm{m\,s^{-1}}$ or 65 kt). The combination of an ice concentration within the precipitation core of the storm and the presence of a rear-inflow jet, as inferred from radar imagery, and the rapid forward motion of the storm contributed to more intense downburst-related winds than the MWPI-derived wind gust potential indicated. Accordingly, regimes favorable for strong downward momentum transfer from flow aloft, and/or enhancement of convective outflow by upscale-growing cold-pool processes (e.g., rear-inflow jet development), may magnify the gust magnitude above what MWPI indicates.

Another challenge to the MWPI used in a downburst forecasting technique is the lower-tropospheric environmental moisture (or relative humidity) profile in proximity to a convective storm of interest. Srivastava (1985) noted that lower environmental relative humidity in the boundary layer, a condition typically associated with an inverted-V thermodynamic profile, has a detrimental effect on downdraft intensity because of the lowering of virtual temperature and the resultant decrease in the virtual temperature deficit between the evaporatively cooled downdraft and the surrounding environment. Thus, in regions where the inverted-V thermodynamic profile is favored, such as the high plains in the United States, a very large ΔDD value will elevate the MWPI, while the environmental virtual temperature in the boundary layer is reduced. The resulting diminished virtual temperature difference between the downdraft and environment will reduce the negative buoyancy of the downdraft and the subsequent downdraft intensity. This condition often results in observed downburst-related wind speeds on the surface that are lower than anticipated by the MWPI wind gust prediction (WGP) algorithm. The dataset employed in the Oklahoma downburst study presented in Pryor (2010) did reveal that the strongest recorded wind gusts ($>25\,\mathrm{m\,s^{-1}}$) were associated with small to moderate ΔDD values between 2° and 12°C. Larger ΔDD values (>15°C) often resulted in weaker downburst-related wind gusts of $20\,\mathrm{m\,s^{-1}}$ or less. In the cases presented in this paper, boundary layer

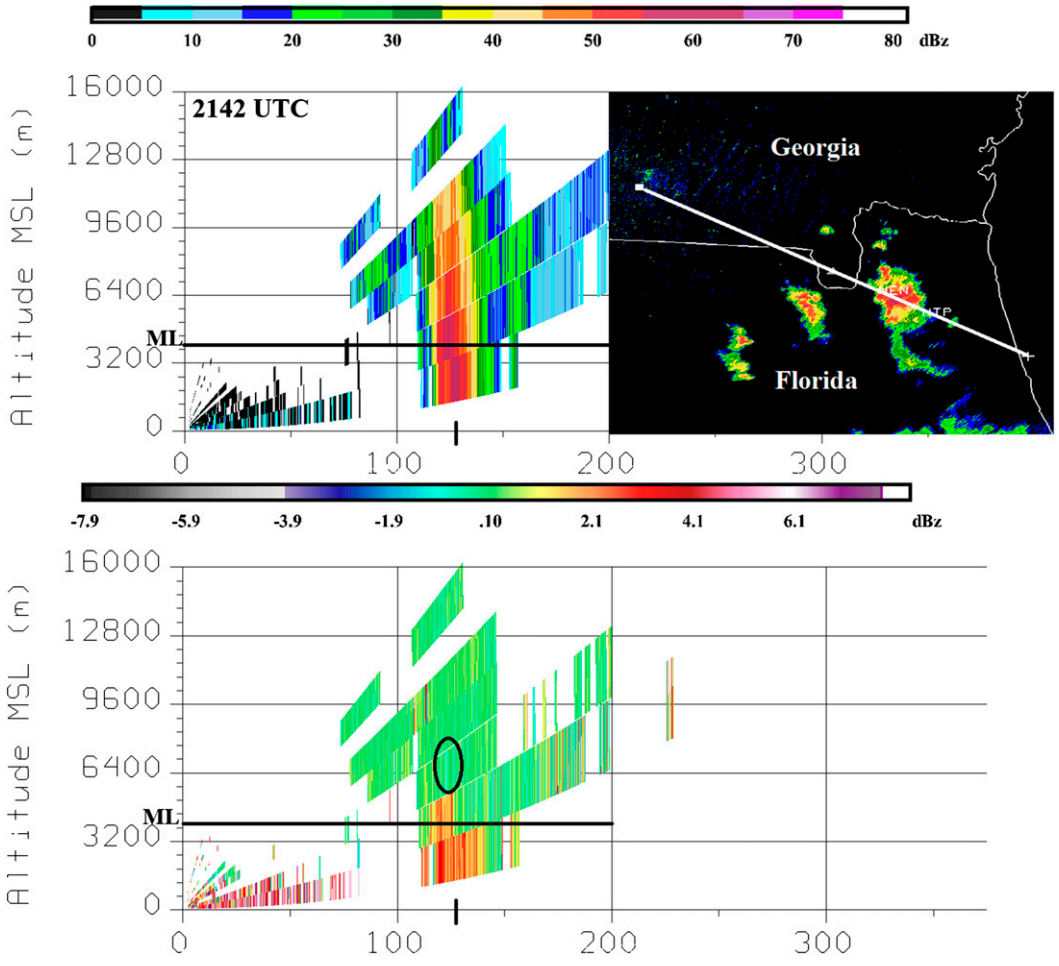

FIG. 13. Moody Air Force Base WSR-88D (top left) Z_h and (bottom) Z_{DR} RHI images at 2142 UTC 10 Jun 2014. The circled region (bottom) indicates the presence of graupel and hail near the ML. The ML was determined by the RAP sounding profile shown in Fig. 11. The black tick at the 125-km range from the NEXRAD site marks the location of a downburst occurrence at NEN. The white line segment (top right) shows a horizontal distance scale of the RHI transect of 200 km.

relative humidity was relatively large (>60%), especially in the lowest 1-km layer of the troposphere, and did not have an apparent diminishing effect on downdraft intensity.

Since both virtual temperature and θ_e are proportional to the moisture content (mixing ratio) of the environment, higher relative humidity in the boundary layer often results in an elevated virtual temperature and θ_e. Thus, in addition to indicating the presence of a midtropospheric unsaturated air layer, large $\Delta\theta_e$ values signify the presence of elevated boundary layer relative humidity as compared to higher layers in the troposphere. Although during the Chesapeake Bay and Florida downburst events the $\Delta\theta_e$ parameter correlated poorly with downburst wind gust magnitude, $\Delta\theta_e$ values were consistently greater than 20°C (not shown). The observed wind gust speeds resulting from downbursts that occurred in the Chesapeake Bay region (excluding the Washington, D.C., event) and in Jacksonville were close to the wind gust potential, as indicated by the MWPI. Therefore, in the situation where environmental virtual temperature is elevated as a result of higher relative humidity, the virtual temperature deficit between the downdraft and the environment is often increased, resulting in enhanced downdraft intensity.

6. Conclusions

As documented in Pryor (2010, 2012, 2014), and shown by statistical analysis, the GOES sounder MWPI product has demonstrated capability in the assessment of wind gust potential over the southern Great Plains and mid-Atlantic coastal regions. Statistical analysis for downburst events that occurred during the 2007–13 convective seasons and recent case studies from the 2013 and 2014

convective seasons demonstrated the effectiveness of the GOES MWPI algorithm, as evidenced by a positive correlation with a high confidence level between MWPI values and measured downburst wind gusts and a low mean error, less than 1 kt, between predicted wind gust speeds derived from the MWPI regression equation and observed wind gust speeds. Furthermore, adding scaling factors to the CAPE, lapse rate, and ΔDD terms in the MWPI formula improved the performance of the product over the Chesapeake Bay region as evidenced by a correlation equal to that found over the southern Great Plains. Validation over the Atlantic coastal region has served to strengthen the functional relationship between MWPI values and downburst wind gust magnitude as well as demonstrating the adaptability of the MWPI algorithm to diverse climatic and geographic regions.

Further validation over geographically diverse regions in the continental United States such as the Florida Peninsula and the Intermountain West and quantitative statistical analysis to assess product performance during the cool season (from October to April) will serve as future work in the development of the GOES MWPI product. Convective storm–generated winds over CONUS during the cool season are often influenced by dynamical factors not accounted for in the MWPI algorithm, including vertical wind shear, and resultant downward horizontal momentum transfer. In addition, the MWPI program has functionality that employs an alternate computation for temperature lapse rate and dewpoint depression difference for the 500–700-mb layer over the higher elevations of the Intermountain West. Future work will detail the validation effort and results of the version of the MWPI product for the western United States, in which the index is calculated for the 500–700-mb layer in regions where the surface elevation is above the 850-mb level. The outcome of additional product validation over the western United States during the warm season and over the CONUS during the cool season will consist of further refinements to the algorithm to increase the adaptability of the MWPI to geographically and climatically diverse regions.

Acknowledgments. The author thanks Dr. Laurie Rokke (chief, Operational Products Development Branch, NOAA/NESDIS), Dr. Xin-Zhong Liang (graduate advisor, Department of Atmospheric and Oceanic Science, University of Maryland, College Park), reviewer Roger Edwards (Operations Branch, NOAA/NWS/SPC), and two anonymous reviewers for their constructive comments and suggestions for this manuscript. The author thanks the Oklahoma and West Texas Mesonets, and WeatherFlow, Inc., for the surface weather observation data used in this research effort. The author also thanks Jaime Daniels (NESDIS) for providing GOES sounding retrieval datasets used in the generation of images displayed in this paper.

REFERENCES

Atkins, N. T., and R. M. Wakimoto, 1991: Wet microburst activity over the southeastern United States: Implications for forecasting. *Wea. Forecasting*, **6**, 470–482, doi:10.1175/1520-0434(1991)006<0470:WMAOTS>2.0.CO;2.

Barnes, S. L., 1994a: Applications of the Barnes objective analysis scheme. Part I: Effects of undersampling, wave position, and station randomness. *J. Atmos. Oceanic Technol.*, **11**, 1433–1448, doi:10.1175/1520-0426(1994)011<1433:AOTBOA>2.0.CO;2.

——, 1994b: Applications of the Barnes objective analysis scheme. Part II: Improving derivative estimates. *J. Atmos. Oceanic Technol.*, **11**, 1449–1458, doi:10.1175/1520-0426(1994)011<1449:AOTBOA>2.0.CO;2.

——, 1994c: Applications of the Barnes objective analysis scheme. Part III: Tuning for minimum error. *J. Atmos. Oceanic Technol.*, **11**, 1459–1479, doi:10.1175/1520-0426(1994)011<1459:AOTBOA>2.0.CO;2.

Battan, L. J., 1973: *Radar Observation of the Atmosphere.* University of Chicago Press, 324 pp.

Brandes, E. A., and A. V. Ryzhkov, 2004: Hail detection with polarimetric radar. Preprints, *11th Conf. on Aviation, Range, and Aerospace Meteorology*, Hyannis, MA, Amer. Meteor. Soc., P5.10. [Available online at https://ams.confex.com/ams/pdfpapers/82033.pdf.]

Bringi, V. N., and V. Chandrasekar, 2001: *Polarimetric Doppler Weather Radar: Principles and Applications.* Cambridge University Press, 636 pp.

Brock, F. V., K. C. Crawford, R. L. Elliott, G. W. Cuperus, S. J. Stadler, H. L. Johnson, and M. D. Eilts, 1995: The Oklahoma Mesonet: A technical overview. *J. Atmos. Oceanic Technol.*, **12**, 5–19, doi:10.1175/1520-0426(1995)012<0005:TOMATO>2.0.CO;2.

Byers, H. R., and R. R. Braham Jr., 1949: *The Thunderstorm.* U.S. Government Printing Office, 297 pp.

Caracena, F., and J. A. Flueck, 1988: Classifying and forecasting microburst activity in the Denver area. *J. Aircr.*, **25**, 525–530, doi:10.2514/3.45617.

Doswell, C. A., III, and D. M. Schultz, 2006: On the use of indices and parameters in forecasting severe storms. *Electron. J. Severe Storms Meteor.*, **1** (3). [Available online at http://www.ejssm.org/ojs/index.php/ejssm/article/viewarticle/11/12.]

Ellrod, G. P., 1989: Environmental conditions associated with the Dallas microburst storm determined from satellite soundings. *Wea. Forecasting*, **4**, 469–484, doi:10.1175/1520-0434(1989)004<0469:ECAWTD>2.0.CO;2.

——, L. Bottos, J. P. Nelson, W. P. Roeder, and M. R. Witiw, 2000: Experimental GOES sounder products for the assessment of downburst potential. *Wea. Forecasting*, **15**, 527–542, doi:10.1175/1520-0434(2000)015<0527:EGSPFT>2.0.CO;2.

Fujita, T. T., 1978: Manual of downburst identification for Project NIMROD. Satellite and Mesometeorology Research Paper 156, University of Chicago, 104 pp.

——, 1985: The downburst, microburst and macroburst. Satellite and Mesometeorology Research Paper 210, University of Chicago, 122 pp.

——, and H. R. Byers, 1977: Spearhead echo and downburst in the crash of an airliner. *Mon. Wea. Rev.*, **105**, 129–146, doi:10.1175/1520-0493(1977)105<0129:SEADIT>2.0.CO;2.

James, R. P., and P. M. Markowski, 2010: A numerical investigation of the effects of dry air aloft on deep convection. *Mon. Wea. Rev.*, **138**, 140–161, doi:10.1175/2009MWR3018.1.

Johns, R. H., and C. A. Doswell, 1992: Severe local storms forecasting. *Wea. Forecasting*, **7**, 588–612, doi:10.1175/1520-0434(1992)007<0588:SLSF>2.0.CO;2.

Knupp, K. R., 1989: Numerical simulation of low-level downdraft initiation within precipitating cumulonimbi: Some preliminary results. *Mon. Wea. Rev.*, **117**, 1517–1529, doi:10.1175/1520-0493(1989)117<1517:NSOLLD>2.0.CO;2.

——, 1996: Structure and evolution of a long-lived, microburst-producing storm. *Mon. Wea. Rev.*, **124**, 2785–2806, doi:10.1175/1520-0493(1996)124<2785:SAEOAL>2.0.CO;2.

Li, Z., J. Li, W. P. Menzel, T. J. Schmit, J. P. Nelson III, J. Daniels, and S. A. Ackerman, 2008: GOES sounding improvement and applications to severe storm nowcasting. *Geophys. Res. Lett.*, **35**, L03806, doi:10.1029/2007GL032797.

Lowry, R., 2014: *Concepts and Applications of Inferential Statistics*. [Available online at http://vassarstats.net/textbook/.]

Menzel, W. P., F. Holt, T. Schmit, R. Aune, A. Schreiner, G. Wade, and D. Gray, 1998: Application of *GOES-8/9* soundings to weather forecasting and nowcasting. *Bull. Amer. Meteor. Soc.*, **79**, 2059–2077, doi:10.1175/1520-0477(1998)079<2059:AOGSTW>2.0.CO;2.

National Transportation Safety Board, 2006: Capsizing of U.S. small passenger vessel *Lady D*, Northwest Harbor, Baltimore, Maryland March 6, 2004. Marine Accident Rep. NTSB/MAR-06/01, 114 pp. [Available online at http://www.ntsb.gov/investigations/AccidentReports/Reports/MAR0601.pdf.]

Pryor, K. L., 2010: Recent developments in microburst nowcasting using GOES. *Proc. 17th Conf. on Satellite Meteorology and Oceanography*, Annapolis, MD, Amer. Meteor. Soc., P9.7. [Available online at https://ams.confex.com/ams/17Air17Sat9Coas/webprogram/Paper174313.html.]

——, 2012: Microburst nowcasting applications of GOES. *Proc. 18th Conf. on Satellite Meteorology, Oceanography, and Climatology*, New Orleans, LA, Amer. Meteor. Soc., 471. [Available online at https://ams.confex.com/ams/92Annual/webprogram/Paper201066.html.]

——, 2014: Downburst prediction applications of meteorological geostationary satellites. *Remote Sensing of the Atmosphere, Clouds, and Precipitation V*, E. Im et al, Eds., International Society for Optical Engineering (SPIE Proceedings, Vol. 9259), doi:10.1117/12.2069283.

——, and G. P. Ellrod, 2004a: Recent improvements to the GOES microburst products. *Wea. Forecasting*, **19**, 582–594, doi:10.1175/1520-0434(2004)019<0582:RITTGM>2.0.CO;2.

——, and ——, 2004b: WMSI—A new index for forecasting wet microburst severity. *Electron. J. Oper. Meteor.*, **5** (3). [Available online http://www.nwas.org/ej/pdf/2004-EJ3.pdf.]

Przybylinski, R. W., 1995: The bow echo: Observations, numerical simulations, and severe weather detection methods. *Wea. Forecasting*, **10**, 203–218, doi:10.1175/1520-0434(1995)010<0203:TBEONS>2.0.CO;2.

Schaefer, J. T., J. J. Levit, S. J. Weiss, and D. W. McCarthy, 2004: The frequency of large hail over the contiguous United States. Preprints, *14th Conf. on Applied Climatology*, Seattle, WA, Amer. Meteor. Soc., 3.3. [Available online at https://ams.confex.com/ams/pdfpapers/69834.pdf.]

Schroeder, J. L., W. S. Burgett, K. B. Haynie, I. Sonmez, G. D. Skwira, A. L. Doggett, and J. W. Lipe, 2005: The West Texas Mesonet: A technical overview. *J. Atmos. Oceanic Technol.*, **22**, 211–222, doi:10.1175/JTECH-1690.1.

Seemann, S. W., E. E. Borbas, R. O. Knuteson, G. R. Stephenson, and H. Huang, 2008: Development of a global infrared land surface emissivity database for application to clear sky sounding retrievals from multispectral satellite radiance measurements. *J. Appl. Meteor. Climatol.*, **47**, 108–123, doi:10.1175/2007JAMC1590.1.

Smith, B. T., T. E. Castellanos, A. C. Winters, C. M. Mead, A. R. Dean, and R. L. Thompson, 2013: Measured severe convective wind climatology and associated convective modes of thunderstorms in the contiguous United States, 2003–09. *Wea. Forecasting*, **28**, 229–236, doi:10.1175/WAF-D-12-00096.1.

Sorbjan, Z., 1989: *Structure of the Atmospheric Boundary Layer*. Prentice Hall, 317 pp.

Srivastava, R. C., 1985: A simple model of evaporatively driven downdraft: Application to microburst downdraft. *J. Atmos. Sci.*, **42**, 1004–1023, doi:10.1175/1520-0469(1985)042<1004:ASMOED>2.0.CO;2.

——, 1987: A model of intense downdrafts driven by the melting and evaporation of precipitation. *J. Atmos. Sci.*, **44**, 1752–1773, doi:10.1175/1520-0469(1987)044<1752:AMOIDD>2.0.CO;2.

Transportation Safety Board of Canada, 2010: Knockdown and capsizing sail training yacht *Concordia* 300 miles SSE off Rio De Janeiro, Brazil. Marine Investigation Rep. M10F0003, 75 pp. [Available online at http://www.bst-tsb.gc.ca/eng/rapports-reports/marine/2010/m10f0003/m10f0003.pdf.]

Wakimoto, R. M., 1985: Forecasting dry microburst activity over the high plains. *Mon. Wea. Rev.*, **113**, 1131–1143, doi:10.1175/1520-0493(1985)113<1131:FDMAOT>2.0.CO;2.

Weisman, M. L., 1992: The role of convectively generated rear inflow jets in the evolution of long-lived mesoconvective systems. *J. Atmos. Sci.*, **49**, 1826–1847, doi:10.1175/1520-0469(1992)049<1826:TROCGR>2.0.CO;2.